Evaluating gust-induced vibrations in high-rise buildings: Insights from in-situ measurements and prediction models[☆]

F.H. Kemper [a] [ID],[*], A.J. Bronkhorst [b], C.P.W. Geurts [b] [ID]

[a] *CWE, RWTH Aachen University, Aachen, Germany*
[b] *TNO, Delft, The Netherlands*

ARTICLE INFO

ABSTRACT

This paper examines gust-induced vibrations in a high-rise residential tower, focusing on the comparison between in-situ measurements and predictions based on current code provisions. Extensive data collected from the New Orleans Tower in Rotterdam — equipped with pressure sensors, accelerometers, and anemometers — was evaluated against predictions derived from the Eurocode and wind tunnel tests. The findings reveal significant discrepancies between measured and predicted accelerations, primarily attributable to inaccuracies in key input parameters rather than limitations of the prediction model itself. The simplified code recommendations fail to account for the effects of neighboring structures and wind directionality. A comprehensive study of aerodynamics force coefficient and structural dynamics were undertaken to assess the prediction models. This study underscores the importance of improving urban wind modeling and incorporating building-specific factors into structural design codes, advocating for the integration of detailed in-situ data and advanced computational techniques to enhance the accuracy of wind-induced vibration predictions in high-rise buildings.

1. Introduction

Wind-induced vibrations are an important factor in the structural design of high-rise buildings. The effect of these vibrations is determined in design practice based on a finite element (FE) model of the building to estimate the global dynamic properties in combination with code calculations or wind tunnel measurements to estimate the dynamic wind effects. Studies comparing the results of these estimated wind effects with in-situ measured effects are not very common, as a long measurement period is required to obtain sufficient measurement data that are even remotely close to serviceability limit state (SLS) design wind conditions. Prior to the 1960s, although there was some recognition that dynamic wind effects existed, such effects were not quantitatively assessed in the design of high-rise buildings. Early studies by, for example, Eiffel (1900), Coyle (1931) and Rathbun (1940) provided the first insights into the response of high-rise structures to dynamic wind effects. In the 1960s, Davenport (1961, 1965, 1967) developed a statistical approach to the assessment of wind loads on structures, which includes the dynamic effects of gusts and vortex shedding. In this approach, these dynamic effects are represented by equivalent static loads that produce the same deflections and stresses.

Van Koten (1971) performed vibration measurements on seven buildings in the Netherlands, ranging in height between 36 and 104 m,

and determined the natural frequencies and damping ratios of these buildings. Van Koten compared the measured vibration levels with the vibration amplitudes calculated with the Gust Loading Factor model by Davenport (1967), and found that the model estimated vibration levels lower than the measured in-situ values. Van Koten (1971) attributed this difference to the horizontal coherence model $e^{-20\frac{nL}{V}}$ applied by Davenport (1967), and states that a better match is obtained with the coherence model $e^{-4\frac{nL}{V}}$ by Eaton (1971).

Jeary (1978) conducted measurements of the dynamic behavior of the 80-meter-high Arts Tower in Sheffield, using both forced vibration tests and wind loading. From the forced vibration tests, he determined the natural frequency, damping ratio, modal mass, and modal stiffness of the first three modes of the building. Comparing the measured stiffness properties with the values used in the design, Jeary observed that the original design values, which only considered the central building core, were significantly smaller than the measured values — 2% in the north-south direction and 17% in the east–west direction. Including the external columns in the analysis accounted for 25% and 60% of the measured stiffness, respectively. He attributed the additional stiffness to internal partition walls and external cladding panels, emphasizing the inadequate understanding of the actual stiffness of buildings at the time.

Jeary also compared the measured accelerations under wind loading with the guidelines provided in Engineering Sciences Data Unit (1976) for calculating along-wind responses. Using the measured modal properties in the calculations, the predicted along-wind responses aligned well with the observed values. Additionally, he noted that the Arts Tower is particularly sensitive to torsional vibrations, which were insufficiently addressed by the estimation methods commonly used during that period.

Dalgliesh et al. (1983) compared in-situ measurements of the along- and across-wind accelerations of the 239-meter-tall Commerce Court Tower in Toronto to values determined from aero-elastic wind-tunnel tests and calculations based on the Canadian National Building Code. The in-situ measurements revealed a decrease in natural frequency, which was accounted for in the code calculations but not in the wind-tunnel measurements. Despite this, the predictions from both the wind-tunnel tests and the code calculations generally aligned well with the measured in-situ accelerations.

The authors also highlighted that the largest discrepancies between in-situ measurements and models occurred for a wind direction significantly influenced by a nearby 285-meter-tall building. They attributed the higher observed vibration levels to potential wake impingement effects caused by this neighboring structure. Furthermore, Dalgliesh et al. (1983) noted the significance of torsional vibrations for the Commerce Court Tower, which result from the building's off-center elastic axis. However, they did not investigate the impact of erroneous predictions of natural frequencies and damping values during the design phase.

The guidelines in codes for calculating wind-induced vibrations make specific assumptions about the mechanisms responsible for the dynamic response. Important assumptions made by the codes that impact the dynamic response include: the reference wind velocity over a 10-minute period is assumed to be stationary; the wind direction is simplified, often considered within a wider sector (typically +/- 45° for aerodynamic coefficients); and the peak factor relation assumes that the building's vibrations follow a Gaussian distribution. By knowledge of the expected extreme amplitudes, it is possible to model the frequency of occurrence of lower amplitudes (Kemper, 2022).

The goal of this study is to evaluate the code provisions from EN 1991-1-4 against the full-scale data obtained at a high rise building. Given the aerodynamic and structural characteristics of the tower under investigation, gust and wake effects are the sole contributors to these vibrations, while vortex-induced vibrations are not relevant due to the high critical velocity of the structure (well above 60 m/s). Therefore, we focus on a concept that predicts these specific types of vibrations, primarily following the Davenport wind loading chain.

To facilitate a meaningful comparison, Section 2 outlines the prediction strategies for gust-induced vibrations, focusing on the most relevant underlying parameters and the challenges associated with predicting them during the planning stage. Section 3 provides a detailed characterization of the building under consideration, its context, wind and structure-related aspects, as well as monitoring conditions. In Section 4, a brief overview of the wind tunnel tests conducted for the New Orleans tower, which were made available for this study, is presented. The key findings from the extensive in-situ dataset are discussed in Section 5. Finally, Section 6 compares the predicted results with statistically extracted measurements.

The novelty of this study lies in its comprehensive approach to evaluating gust-induced vibrations in high-rise buildings, utilizing an extensive dataset that surpasses previous real-world cases. The dataset, derived from long-term monitoring of the New Orleans Tower, represents an unprecedented volume of in-situ measurements, including wind speeds, pressure distributions, and acceleration data collected over several years.

This rich data resource not only enables a robust comparison between predicted and measured vibrations but also serves as a valuable reference case for future studies. In particular, the dataset is intended to facilitate the development and validation of adjusted prediction methods, incorporating high-fidelity numerical simulations, wind tunnel tests using High-Frequency Force Balance (HFFB) models, and high-density pressure measurements.

2. Prediction of gust-induced vibrations

2.1. Wind loading chain

The stochastic wind loading of building structures can be described with a frequency-based approach, as defined by the Davenport wind loading chain (Davenport, 1965). This chain relates key aspects that determine the wind loads on building structures: the wind climate, the exposure, the building aerodynamics and the structural response. Due to its comprehensible and physical description of the stochastic wind load, the wind loading chain forms the basis for most wind loading codes worldwide.

This paper uses the parameters and guidelines prescribed in NEN-EN 1991-1-4 (Netherlands Standardization Institute, 2011), which is the Dutch translation of EN 1991-1-4 and together with the added provisions in the Dutch National Annex (Netherlands Standardization Institute, 2023) applies in the Netherlands. The provisions in these documents are used for determining wind-induced vibrations as an example for the comparison of code provisions with the in-situ measurements on the residential building the New Orleans (see Section 3.1). The standard deviation of the in-wind acceleration amplitude ẍ can be determined as:

$$\sigma_{\ddot{x}}(z) = \rho \cdot I_v(z) \cdot v_m^2(z) \cdot c_D \cdot R \cdot \frac{K_y \cdot K_z \cdot \Psi(z)}{\mu_{ref} \cdot \Psi_{max}} \tag{1}$$

where $\sigma_{\ddot{x}}(z)$ is the standard deviation of the characteristic along-wind acceleration at height z, derived based on a frequency based approach (including gust spectrum, aerodynamic and mechanical admittance). The parameters in the right hand part of Eq. (1) are arranged in order of the wind loading chain links (climate, exposure, aerodynamics, and structure). Where ρ is the density of air, I_v the turbulence intensity, v_m the mean wind speed, c_D the aerodynamic drag coefficient, and R represents the resonance effect based on the gust spectrum and structural dynamic properties. The fraction in Eq. (1) represents further structural contributions, which can be assumed independent of wind conditions and aerodynamic effects. $\Psi(z)/\Psi_{max}$ is the relative mode shape factor, K_x, K_y are mode shape factors, and μ_{ref} the equivalent mass per area.

Some of the involved parameters may be determined by in-situ measurements. Their identification and the comparison of results obtained by such data with results obtained using simplified assumptions are discussed in the following paragraphs.

As a criteria for the appraisal of serviceability, NEN-EN 1991-1-4 (Netherlands Standardization Institute, 2011) uses the characteristic peak along-wind acceleration of the structure:

$$\ddot{x}_{p,EN}(z) = \sigma_{\ddot{x}}(z) \cdot k_p(n_1) \tag{2}$$

In the context of Gaussian random processes, the probability distribution of extreme values can be derived from the assumption that the structural response follows a stationary normal distribution. The peak factor k_p accounts for the expected ratio between the maximum response during a finite duration T and its standard deviation. Following the extreme value statistics for Gaussian processes (e.g., Netherlands Standardization Institute, 2011; Davenport, 1964), the peak factor is expressed as:

$$k_p = \max \left\{ \sqrt{2 \ln(\nu T)} + \frac{0.6}{\sqrt{2 \ln(\nu T)}}; \ 3.0 \right\} \tag{3}$$

where ν is the zero-upcrossing frequency of the response (here taken as the fundamental natural frequency n_1) and $T = 600$ s is the reference duration of the wind event.

Eqs. (1) and (2) represent "Method 2" of the Eurocode 1 (distributed as NEN-EN 1991-1-4 (Netherlands Standardization Institute, 2011) in the Netherlands). According to Steenbergen et al. (2012), this procedure offers greater accuracy compared to "Method 1". Although it is based on the same theory, it simplifies the consideration of mode shapes

by taking them outside the integral in the aerodynamic admittance calculation. This simplification can lead to underestimations, particularly in the resonance response of tall, slender buildings. Consequently, all subsequent input variables in this paper are calculated using "Method 2".

With respect to in-situ measurements and the overall validation of Eq. (2), particular attention is given to the wind and aerodynamic-related parameters, as they are presumed to carry the highest degree of uncertainty. In the following subsections, the different influencing aspects are described in a general way. In Section 3.1, we introduce specific values of the investigated high-rise structure for all relevant parameters based on a typical design stage study using the code recommendations. Additionally, we introduce enhanced values based on measurements in order to see the influence on the design predictions (Section 6).

2.2. Wind climate and exposure

The exposure is expressed by the roughness length z_0. For our study we have estimated exposure categories, represented by z_0 for wind 30 ° sectors based on visual analysis of the surrounding (typical method in a planning stage). The mean wind velocity is described based on the assumed exposure category as follows:

$$v_m(z) = c_r(z) \cdot c_o(z) \cdot v_b$$
$$= 0.19 \cdot \left[\frac{z_0}{z_{0,II}}\right]^{0.07} \cdot \ln\left[\frac{z}{z_0}\right] \cdot c_o(z) \cdot c_{dir} \cdot c_{prob} \cdot v_{b,0} \quad (4)$$

where $z_{0,II} = 0.05\,\text{m}$ is the reference roughness according to Netherlands Standardization Institute (2011) and z the height above ground level. The fundamental value of the basic wind velocity, $v_{b,0}$, is the characteristic 10-minutes mean wind velocity, irrespective of wind direction and time of year, at $z = 10$ m above ground level in open country terrain. The parameters c_o, c_{dir} allow further modifications – however, the recommended values are all equal to 1.0 and therefore neglected. The probability factor c_{prob} allows for the adjustment of the return period to values other than the standard 50 years. The turbulence intensity is calculated to:

$$I_v(z) = \frac{\sigma_v}{v_m(z)} = \frac{k_I}{c_0(z)\ln(z/z_0)} \quad (5)$$

The estimation of roughness length z_0 introduces considerable uncertainty, particularly in densely urbanized areas. Real data on urban wind flow is scarce, making it challenging to precisely quantify the influence of surrounding structures. In typical prediction studies, addressing this uncertainty would involve varying roughness parameters within reasonable ranges and analyzing the resulting impact on acceleration predictions. However, such a comprehensive approach is rarely undertaken, as it requires extensive experimental or computational effort.

In dense urban environments and for high-rise buildings, such as the New Orleans Tower, the conditions to neglect the effect of wake turbulence due to neighboring structures are typically not met. According to NEN-EN 1991-1-4 (Netherlands Standardization Institute, 2011), the effect of increased turbulence in the wake of nearby structures should be considered for slender buildings ($h/d > 4$). Wake turbulence can be disregarded if either the distance between two structures is greater than 25 times the cross-wind dimension of the upstream building, or if the natural frequency of the downstream building is above $f = 1.0$ Hz. NEN-EN 1991-1-4 (Netherlands Standardization Institute, 2011) recommends wind tunnel tests or specialist advice when neither the distance condition nor the natural frequency condition is fulfilled.
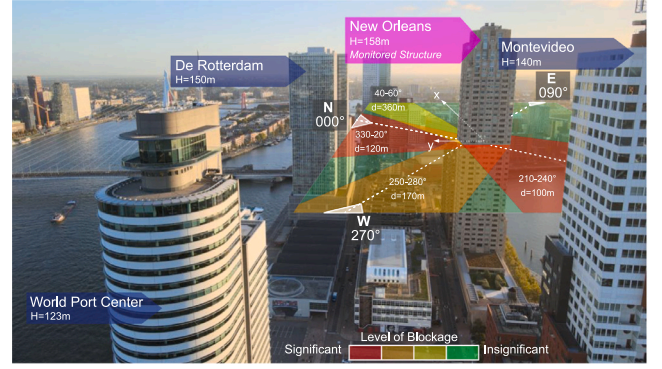

Fig. 1. Location of the New Orleans Tower and adjacent buildings in the center of Rotterdam, the Netherlands. Description of wind directions with respect to the level of blockage.

2.3. Building aerodynamics

The influence of building aerodynamics is either described based on external pressure coefficients c_{pe} which reflect the distribution of the wind effect over the surface or condensed in aerodynamic force coefficients c_f for relevant directions (either in a building reference system: $c_{f,x}$, $c_{f,y}$, or in a wind reference system: c_D, c_L).

In real-world structures, several factors can introduce uncertainty due to the simplified descriptions provided in standards. These factors include surface roughness, Reynolds number effects, wind direction influence, and deviations in geometry. In the planning stage, significant improvements of the predictions can be achieved with wind tunnel studies.

For the simplified considerations in the planning stage, typically standardized force coefficients are used, e.g. for rectangular cross-section (flow perpendicular to one side of the cross-section) according to NEN-EN 1991-1-4 (Netherlands Standardization Institute, 2011). A consideration of directional effects is normally not possible, and the influence of neighboring structures is neglected completely. For our study, besides in-situ data, results of a wind tunnel test are available, providing directional force coefficients which also consider the influence of adjacent buildings.

2.4. Structural properties and resonance response

The structural response of high-rise towers is primarily characterized by the dynamic properties, which are dependent on the distribution of stiffness and mass along the height of the tower, the damping behavior of both the tower and its support, and the rigidity of the support structure. It is challenging to predict these influences accurately in the planning stage, as the damping properties and the stiffness-contributing effects of secondary components must often be assessed based on assumptions. Moretti et al. (2022) made a comparison of structural parameters applied in the design of the New Orleans tower and those obtained using the measured modal properties. In our calculations, we use both structural parameter sets (see Section 3.1) to study the influence on the vibrations' prediction.

With respect to Eq. (1), the resonant part of the structural response R is another input parameter. It is determined (again following the Davenport Wind load chain) based on the gust spectrum, aerodynamic and mechanical admittance:

$$R^2 = \frac{\pi^2}{2\delta} S_L K_s \quad (6)$$

where δ is the logarithmic damping decrement and S_L the spectral density of the gust spectrum at the natural frequency of the structure. K_s

represents the joint acceptance function which considers the gust correlation over the length considering the structural mode shape. For further details we refer to NEN-EN 1991-1-4 Netherlands Standardization Institute (2011) and Steenbergen et al. (2012).

2.5. Relation between the variability of wind speed, wind force and acceleration

For the analysis of in-situ data, it is often necessary to convert measured quantities in cases where the desired values cannot be directly obtained. Furthermore, identifying correlations is often a key objective to improve or validate models. To support this effort, several assumptions are introduced below to aid in data interpretation.

Based on strip theory, the drag force $F_D(t)$ acting on a structure is defined as:

$$F_D(t) = \int_0^h c_D(z) \, q(z,t) \, b \, dz \tag{7}$$

where $q(z,t) = \frac{1}{2}\rho v^2(z,t)$ is the time-dependent gust velocity pressure at height z, ρ is the air density, $c_D(t)$ is the time-dependent aerodynamic drag coefficient, and b the associated reference dimension (here, the cross-wind width). For a cross-section with unique shape over height, this simplifies to:

$$F_D(t) = c_D \, b \int_0^h q(z,t) \, dz \tag{8}$$

The integral formulation for the height dependent gust velocity pressure may be further simplified according to NEN-EN 1991-1-4 (Netherlands Standardization Institute, 2011), by the introduction of a reference height z_s, which is based on the work by Solari and Kareem (1998) on the equivalent wind spectrum technique for dynamic calculations on structures. This approach assumes that the gust velocity pressure can be represented by a single effective value at height z_s, thus transforming the integral expression into a simplified form:

$$F_D(z_s, t) = c_D \, b \, h \, q(z_s, t) = c_D \, A \, q(z_s, t) \tag{9}$$

for tall buildings, $z_s = 0.6 \, h$ is proposed in Solari and Kareem (1998), which is also specified in NEN-EN 1991-1-4 (Netherlands Standardization Institute, 2011). When normalizing the drag force using the mean gust velocity pressure, $\bar{q} = \frac{1}{2}\rho \bar{v}^2$, the drag coefficient is computed as:

$$c_D(t) = \frac{F_D(z_s, t)}{\bar{q}(z_s)A} \tag{10}$$

The reference area A is the projected frontal area of the building, which is a standard approach when defining drag coefficients in the wind coordinate system. In this formulation, the variability of $F_D(z_s \, t)$ is fully mapped to $c_D(t)$ because the mean gust velocity pressure $\bar{q}$ is treated as constant (assuming non-linear effects and vortex-shedding are negligible). Under this assumption, the time-dependent fluctuations in $c_D(t)$ directly reflect the aerodynamic and turbulence-induced variability in $F_D(z_s, t)$.

The turbulence intensity, I_v, is defined as:

$$I_v = \frac{\sigma_v}{\bar{v}} \tag{11}$$

where σ_v is the standard deviation of the wind velocity, and $\bar{v}$ is the mean wind velocity. Using first-order linearization, the standard deviation of the gust velocity pressure σ_q is proportional to the turbulence intensity at a single point:

$$\sigma_q = \frac{\rho}{2} \cdot (2\bar{v}) \cdot \sigma_v = 2\bar{q} \cdot I_v \tag{12}$$

This relationship can be applied to the cross-section of a component being flowed around; however, a loss of correlation must be taken into account. If the variability of $F_D(t)$ is entirely transferred to $c_D(t)$, the standard deviation σ_{c_D} scales as:

$$\frac{\sigma_{F_D}}{F_D} \rightarrow \frac{\sigma_{c_D}}{c_D} \approx 2(1-\alpha)\frac{\sigma_v}{\bar{v}} = 2(1-\alpha)I_v \tag{13}$$

Fig. 2. New Orleans Tower, H=158 m, located in Rotterdam, the Netherlands. View of the structured facade.

where α is a coefficient representing the loss of correlation between the fluctuations of the incoming wind velocity and the fluctuations of the drag coefficient. This loss of correlation arises because the drag force results from the surface-integrated wind pressure, which is an effect of the turbulent velocity fluctuations in the approaching flow as well as the building induced turbulence. Hence, the variation coefficient of the drag force can be used to estimate the prevailing turbulence intensity in the approaching wind flow, as long as a reasonable assumption for α can be justified based on data.

The along-wind acceleration at a specific height $\ddot{x}(z)$ is proportional to the applied drag force F_D, as described by Newton's second law. Under varying wind conditions, this proportionality holds only if the composition of the load spectrum remains unchanged (e.g. no vortex-induced effects). Under this assumption, and further assuming no significant influence from altered correlation patterns, a linear relationship between the drag force and the resulting acceleration can be reasonably established. Consequently, the standard deviation of the acceleration, $\sigma_{\ddot{x}}(z)$, can also be assumed proportional to the standard deviation of the drag force coefficient σ_{c_D}.

3. Parameters and set-up of in-situ measurements

3.1. Building and context

The New Orleans (NO) Tower (Fig. 1), situated on a peninsula in the Nieuwe Maas River in Rotterdam, stands at a structural height of $h = 158$ meters and dimensions of 29 m in both depth and width. Its cross-section is predominantly square, with slight façade offsets contributing to its architectural form (Fig. 2). The façade consists of natural stone slabs, each with an area of $A = 1 \, m^2$, separated by narrow gaps of $e = 10$ mm.
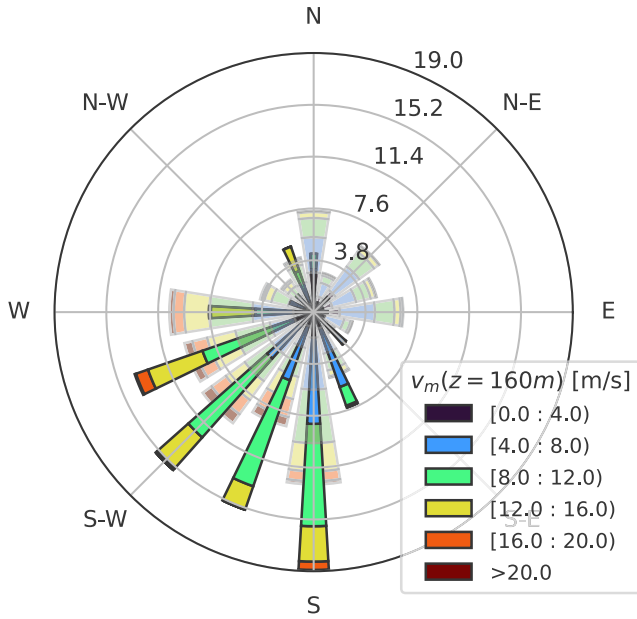
Fig. 3. Wind speeds measured at RTM, upscaled to height of roof top (wide bars) and directly measured at the New Orleans Tower with an ultrasonic probe (shaded bars).

Fig. 4. Roughness conditions in the surrounding of the New Orleans Tower and 30° sectors.

3.2. Wind characteristics

Wind velocity data from both a wind station at Rotterdam-The Hague airport (RTM) and an anemometer on top of the New Orleans Tower are used. First, the data monitored by an ultrasonic probe, located on the roof top (Fig. 5(b)) is available for the complete data period. Second, wind speed data is available from the RTM airport for the same time period (hourly mean wind speeds and directions). From the original RTM sensor height, this data has been upscaled to $z = 158$ m based on Eq. (4). Fig. 3 shows wind roses of mean wind velocity from both sources in comparison. With respect to the measured velocities, the results are quite comparable for the undisturbed directions (cf. Fig. 1). For the disturbed sectors, remarkable differences can be observed. Additionally, due to the positioning of the ultrasonic probe on the roof, especially flow from north-east is disturbed and deviated. As a result, the directional frequencies of occurrence deviate compared to the data of the RTM station (see Fig. 4).

For the analysis of monitored data (like pressure and acceleration), in this study the wind data of (RTM) is used at relevant height z_{ref} using Eq. (4).

The roughness conditions surrounding the building can be evaluated using the satellite image provided in Fig. 1, covering all wind sectors. Within a radius of 2000 m, the area exhibits significant variability in surface roughness, ranging from smooth water surfaces to densely built-up areas with an average building height exceeding 15 m. For most wind directions ($\Phi = 240° - 260°$), a roughness length of $z_0 = 1.0$ m is estimated. In the WSW direction, however, the terrain would reflect a smoother roughness length of $z_0 = 0.05$ m as the wind approaches from the river. Due to the narrow extent of this smoother terrain and the expected mixing within the three-dimensional flow field, the resulting boundary layer is not significantly influenced by the reduced roughness in that direction and the roughness length is assumed to $z_0=1.0$ m for all wind directions.

Based on the outlined assumptions for the roughness length z_0, key parameters such as extreme wind speed, turbulence intensity, and the integral length scale of turbulence can be derived (see Section 2).

To enhance the understanding of roughness effects, this study includes data from three anemometers located near the New Orleans Tower, including one on the rooftop. These measurements will provide valuable insights into the wind profiles influenced by surrounding roughness. The inclusion of this data in future analyses will enable a more precise characterization of urban wind flow and its impact on gust-induced vibrations but is part of ongoing analysis.

Further considerations as realistic roughness estimation or a detailed conversions of wind speed measured at (RTM) towards the (NO) tower have not been made yet. For a later analysis, it is aimed to consider measured wind speeds of a high-rise structure located north-north-west to the tower where another monitoring system is running. In that case, the wind anemometer on top is less disturbed and provides higher turbulence resolution.

Due to a slenderness of $h/d = 5.44$ and structural Eigenfrequencies significantly below $f = 1$ Hz (see Section 5.3), the criteria to neglect wake effects acc. to NEN-EN 1991-1-4 (Netherlands Standardization Institute, 2011) are not met (cf. Section 2.2).
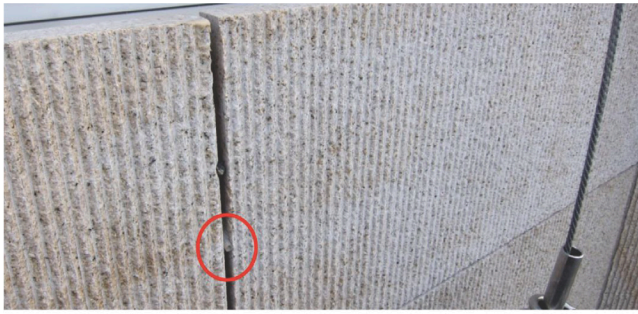
3.3. Time period, time sequences and sampling rate

This study analyses data obtained from 01/2012 to 12/2020. The sampling rate of the data is $f_s = 20$ Hz. All data were converted from the original text-based format into an SQL database, enabling fast and efficient filtering. A second database was set-up containing the (RTM) meteorological data in a height of $z = 10$m. This database was used to filter time stamps with significant wind velocities (in this study, $v_{cond.}(z = 114.6$ m$) \geq 8$ m/s) and to filter the measured events according to the prevalent (undisturbed) wind speed.

For all analyses, an additional binning of wind direction sectors has been performed ($\Delta\Phi = \pm10°$). For each wind sector, time series with a length of 10 min (±5 min around the hourly timestamp) have been used for deeper statistical analyses. The above-mentioned conditions are met for a set of 130,885 datasets within the complete measurement period, representing a coherent time period of 908 days, which is roughly 28% of the total observation time.

3.4. Pressure taps and sensors, anemometer

At a height of $z = 114.6$ m (34th floor), in total 40 pressure transducers were installed: 20 measuring external pressures near the slab openings and 20 measuring cavity pressures at the center of the slab's backside. The positions of the external pressure taps are shown in Fig. 6(a). Flexible tubes (6 mm internal diameter, 4 m maximum length) connect the pressure taps to transducers located on balconies, minimizing resonance effects. Laboratory tests determined the amplification factor for different tube lengths, allowing for a correction to the

(a) Detail of a pressure tap in the facade

(b) Ultrasonic anemometer on the roof top

Fig. 5. Examples of instrumentation of the New Orleans tower for the measurement campaign.

(a) Location of pressure sensors

(b) Locations and directions of accelerometers

Fig. 6. Arrangement of Sensors and definition of structural and wind related coordinate systems.

pressure signals for the interpretation of dynamic amplitudes. A reference pressure vessel inside the building connects all transducers and includes a shiftable valve for regular offset measurements (van Bentum and Geurts, 2015). Offset values are stored for each measurement run to enable accurate corrections. Each measurement duration is 10 min. In addition to the pressure measurements, an ultrasonic anemometer was installed on the roof at a height of 160 m (Bronkhorst and Geurts, 2020).

3.5. Acceleration sensors

Two 1D and a 2D accelerometer are installed at a height of 114.6 m (34th floor). The arrangement of the sensors with respect to position and measurement direction is shown in Fig. 6(b). The arrangement allows interpretation of transversal and torsional motion of the building. Accelerometer which are not installed at the center of mass, always detect a superposition of transversal and rotational components. For the analyses, the center of mass is assumed at the geometrical center. Under this assumption, the translational acceleration over the buildings' main axes derives to:
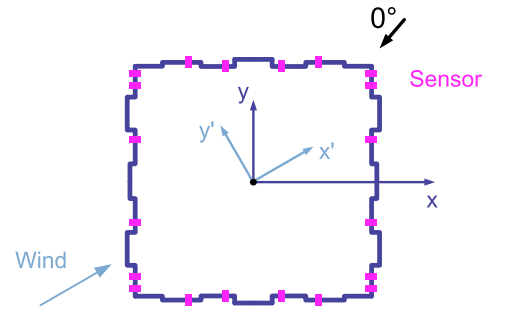
$$\begin{bmatrix} \ddot{x} \\ \ddot{y} \end{bmatrix} = \begin{bmatrix} \frac{L_4}{L_2+L_4} & \frac{L_2}{L_2+L_4} & 0 & 0 \\ 0 & 0 & \frac{L_3}{L_1-L_3} & -\frac{L_1}{L_1-L_3} \end{bmatrix} \cdot \begin{bmatrix} \ddot{a}_2 \\ \ddot{a}_4 \\ \ddot{a}_1 \\ \ddot{a}_3 \end{bmatrix}$$ (14)

Where $\ddot{a}_i$ denotes the measured acceleration signals from sensors 1 to 4, and L_i represents the distance of each sensor from the center of geometry, as shown in Fig. 6(b). The resulting acceleration $\ddot{r}_c$ at the center can be calculated as:
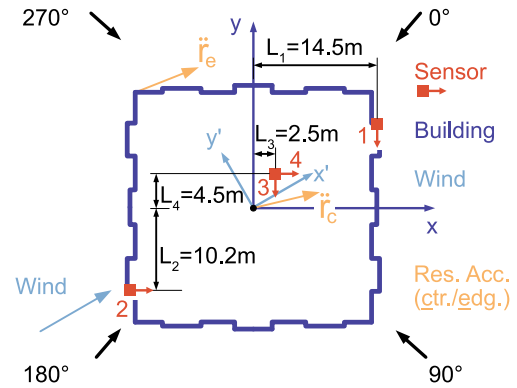
$$\ddot{r}_c = \sqrt{\ddot{x}^2 + \ddot{y}^2}$$ (15)

Angular acceleration due to torsional vibration can be identified using:

$$\ddot{r}_t = \left| \arctan\left(\frac{\ddot{a}_1 - \ddot{a}_3}{L_1 - L_3} \right) \right|$$ (16)

while the most unfavorable acceleration at the farthest edge is calculated as:

$$\ddot{r}_e = \ddot{r}_c + \ddot{r}_t \cdot e$$ (17)

With respect to comfort criteria $\ddot{r}_e$ is more relevant, while for the interpretation of the structural response the components in the buildings' main axes x, y might be more relevant.
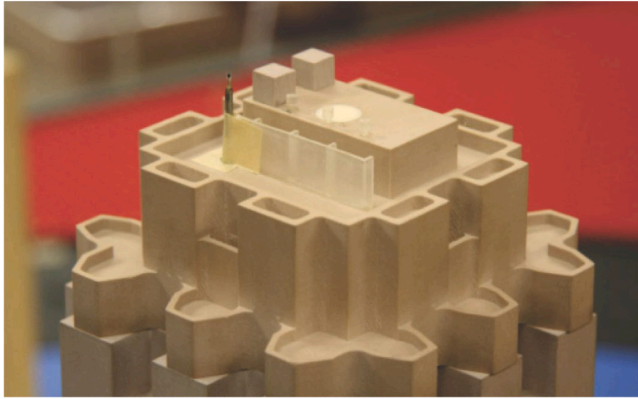
4. Wind tunnel tests

Data from a previous wind tunnel test of the New Orleans tower, conducted at TNO's (Dutch research institute) atmospheric boundary layer wind tunnel in Apeldoorn (Koster et al., 2014), was made available for the current study. These measurements were performed to determine the wind loads on the facade elements of the tower and therefore were set up in accordance with the Dutch guideline for wind tunnel measurements CUR 103 (Anon, 2005). This guideline is specifically mentioned by the Dutch National Annex to the EN 1991-1-4 (Netherlands Standardization Institute, 2023) for the determination of wind loads through wind tunnel measurements. A 1:250 geometrical scale model represented the tower and surrounding buildings within a 375 m radius (see Fig. 7). The model, approximately 60 cm tall, was tested in a boundary layer with a thickness of 1.3 m at the turntable center, ensuring realistic flow conditions. Terrain roughness was initially identified as $z_0 = 1.6$ m (full-scale) for most of the area surrounding the tower within a 5 km radius. However, the immediate vicinity, dominated by water, had a much lower roughness length of $z_0 = 0.001$ m.

To ensure a conservative assessment of local wind loads on the façade elements, the Dutch guideline for wind tunnel measurements

(a) Complete wind tunnel model

(b) Detail of roof situation

Fig. 7. New Orleans tower and directly adjacent buildings in the boundary layer wind tunnel at TNO, the Netherlands.

Fig. 8. Exemplary mean pressure distribution based on wind tunnel test for a flow direction of $\Phi = 270°$.

(Anon, 2005) was followed by adopting a reduced full-scale roughness length of $z_0 = 0.03$ m. This value increases both the reference gust velocity pressure and the magnitude of façade pressure coefficients, thereby leading to higher design wind loads. Such an approach is consistent with the intent of standards including NEN-EN 1991-1-4 (Netherlands Standardization Institute, 2011) and ASCE 7-22 (Anon, 2022), where smoother terrain categories are regarded as conservative, since they yield the largest structural actions for a given basic wind velocity.

In the closed-section tests, the blockage ratio was direction-dependent, varying between 3.5% for $\Phi = 45°$ and 225°, and 6.5% for the most unfavorable wind directions ($\Phi = 135°$ and 315°). Although guidelines generally recommend keeping blockage below about 5% to minimize aerodynamic interference (Simiu and Scanlan, 1996; Buresti, 1981; Antoine and Olivari, 2009), values up to 7%–10% are often reported as still acceptable, especially when blockage corrections are small and the test configuration does not induce strong confinement effects. In this study, the blockage level therefore remains within an acceptable range, while future tests are planned at smaller scale in an open-section facility with more realistic roughness and a maximum blockage of about 5%.

Pressure measurements were conducted at 88 taps distributed across four floors of the New Orleans model: the 24th, 30th, 35th, and 38th floors. These taps captured pressures on two full-width sides and at corners on the other two sides, with additional runs performed at a 180° model rotation to determine the full circumference distribution. Sampling was conducted using 32-channel analog pressure modules with an accuracy of ± 5 Pa, corrected for tubing effects. Measurements were taken for 24 wind incidence angles at 15° increments, with a sampling rate of 400 Hz over a 20.4-second period. The selected

duration corresponds to a full-scale time period of 3600 s. Fig. 8 shows exemplary the mean external pressure coefficients $c_{pe,m}$, measured at the 35th floor. The undisturbed wind velocity at the building height was 13.8 m/s, measured with a pitot-static tube. These measurements, along with the conservative terrain roughness assumption, provided a robust dataset for evaluating façade pressures and their distribution under conservative flow conditions.

Analyses have been made for all flow direction, highest positive pressure coefficients have been found up to $c_{pe,m} = +0.8$, while the negative pressure coefficients have been found to $c_{pe,m} = -1.2$ Corresponding mean drag and mean lift forces have been analyzed and maximum mean drag has been found at $c_D = 1.5$, while $c_L = \pm 0.5$.

According to NEN-EN 1991-1-4 (Netherlands Standardization Institute, 2011), the almost squared cross section under perpendicular flow towards one surface has a drag force coefficient of $c_{D,0} = 2.15$. Taking into account the reduction factor for slenderness $\psi_{lambda} = 0.68$, an effective force coefficient of $c_{D,EN} = 1.46$ is derived.

Both the wind tunnel data and the values proposed by the standard are used for comparison with in-situ results (see Section 5).

5. Results of in-situ measurements

5.1. Average surface pressure

Pressure coefficients have been derived using RTM wind speeds, upscaled to a height of $z = 114.6$ m, using Eq. (5) and the roughness conditions of Section 3.1. For the analyzed average pressure coefficients, the distributions show reasonable positive pressure coefficients (indicating overpressure), but lower negative pressure coefficients (indicating underpressure) compared to wind tunnel data. It is aimed to analyze the pressure data with smaller time sequences to account for possible changing wind conditions within the 10 min time period.

5.2. Aerodynamic forces

In Fig. 8, a visualization of the external pressure distribution across the building's cross-section is shown. The visualization was generated
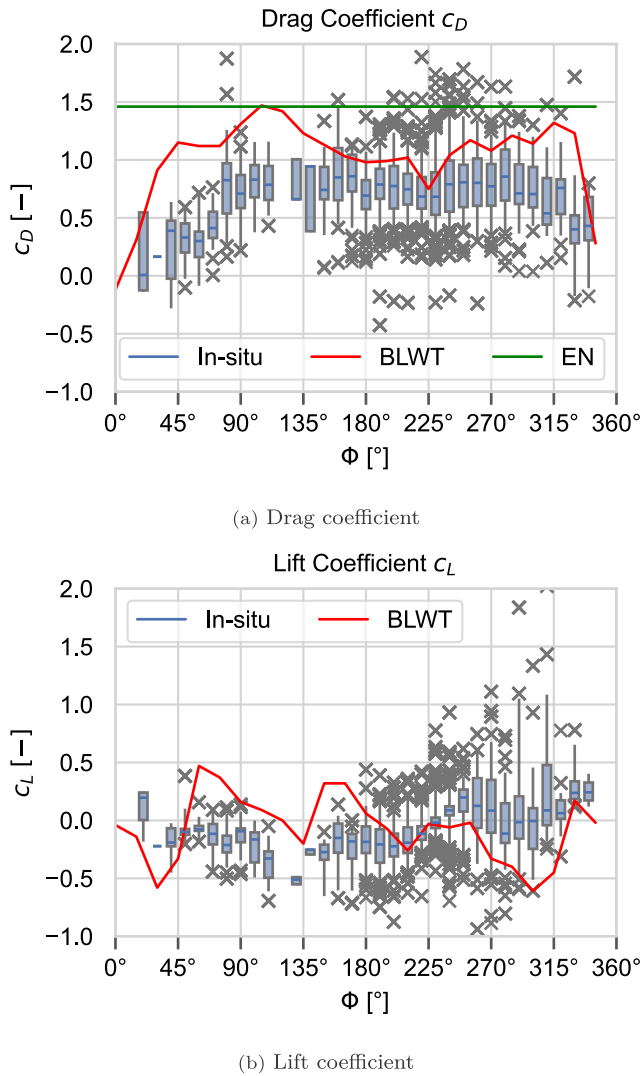
Drag Coefficient c_D

(a) Drag coefficient

Lift Coefficient c_L

(b) Lift coefficient

Fig. 9. Force coefficients as a result of surface integration for all measured pressure data and comparison to BLWT tests in "smooth" terrain (see Section 4) and EN model (see Section 3.2), where applicable.

using matrix operations to project the measured data onto the building geometry (tap-to-wall matrix). The same computational framework is utilized to integrate the pressure over the cross-sectional surfaces, accounting for each orientation within the building's x–y coordinate system. As a result, the force coefficients $c_{f,x}$ and $c_{f,y}$ are calculated. The drag and lift force coefficients, c_D and c_L, are derived based on the mean wind direction (RTM) within each 10-minute interval, using a transformation of the building-specific force coefficients to align with the wind direction. The method was applied for both, BLWT and in-situ data. The results are plotted in Fig. 9 as box plots, with whiskers representing the 5%–95% quantiles and outliers marked with 'x'.

c_D and c_L are defined in the wind coordinate system. The observed tendency of c_D to approach zero for certain wind directions (Φ) and missing values for the 0°-direction can be attributed to significant upstream blockage caused by neighboring structures. This effect occurs when the wind approaches from angles where adjacent buildings shield the New Orleans Tower from direct wind exposure. As a result, the effective wind pressure on the building facade is substantially reduced. Please refer to Fig. 1 for a visualization of the blockage situation.

As shown in Fig. 9, this reduction in c_D for specific wind directions is consistently observed in both full-scale measurements and wind tunnel tests.

The Eurocode generally assumes a perpendicular wind incidence when specifying the drag coefficient, without accounting for directional variability. This simplification may lead to discrepancies when the building is partially shielded by surrounding structures, highlighting the importance of considering site-specific aerodynamic conditions.

The overall wind forces cannot be determined with the current monitoring system, as the pressure analysis is restricted to a single horizontal slice of the building. However, the sectional force coefficients presented here can provide valuable input for refining normative procedures or validating BLWT and CFD results (see Section 5.2).
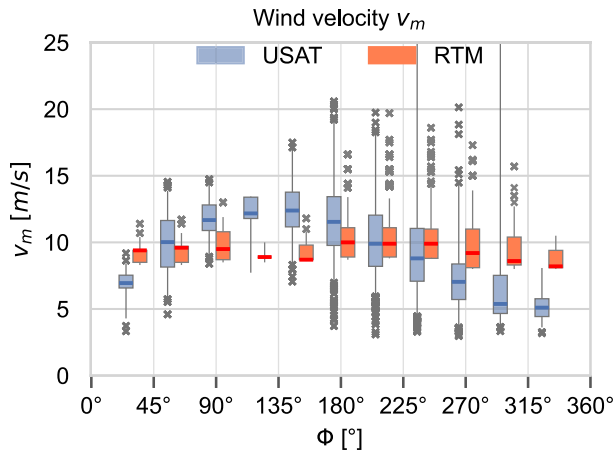
5.3. Structural properties

According to Moretti et al. (2022), the measured structural frequencies in the first mode shapes are nearly identical over both axes ($f_x = 0.291$ Hz and $f_y = 0.282$ Hz). These values are considered as reference values for the structural frequencies. Besides, data from the design stage for that building are available ($f_x = 0.189$ Hz and $f_y = 0.212$ Hz), showing a significant underestimation of the natural frequencies (which results in a conservative result for the resonant response). The structural mass applied in the design model was $\rho = 500$ kg/m^3, while the mass analyzed in Moretti et al. (2022) is about $\rho = 475$ kg/m^3. The damping applicable according to NEN-EN 1991-1-4/NB (NEN, 2023) is $\delta_x = \delta_y = 0.11$ for both modes, in which both structural and aerodynamic damping are considered. In Bronkhorst and Geurts (2020), lowest damping ratios $\zeta_x = 0.8\%$ and $\zeta_y = 0.9\%$ have been analyzed based on the measurements, which correspond with logarithmic damping decrements of $\delta = 0.05$ and $\delta = 0.06$. The influence of estimated structural properties and realistic values on the acceleration prediction is shown in Section 6.
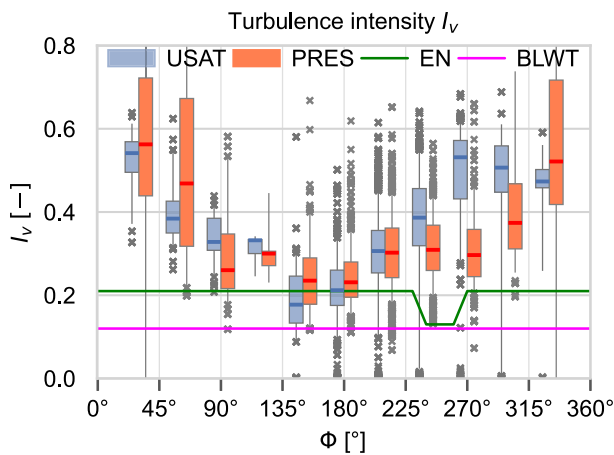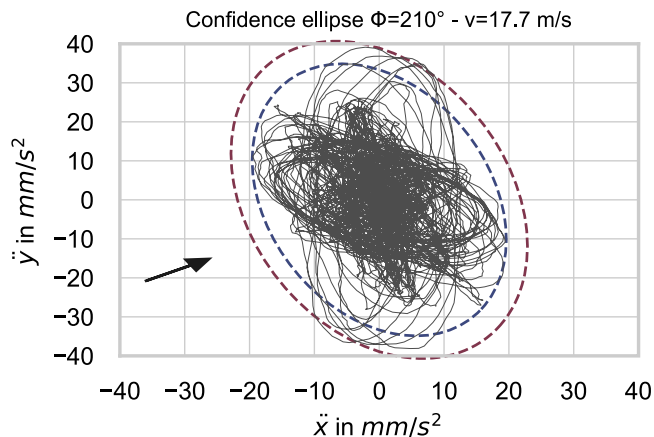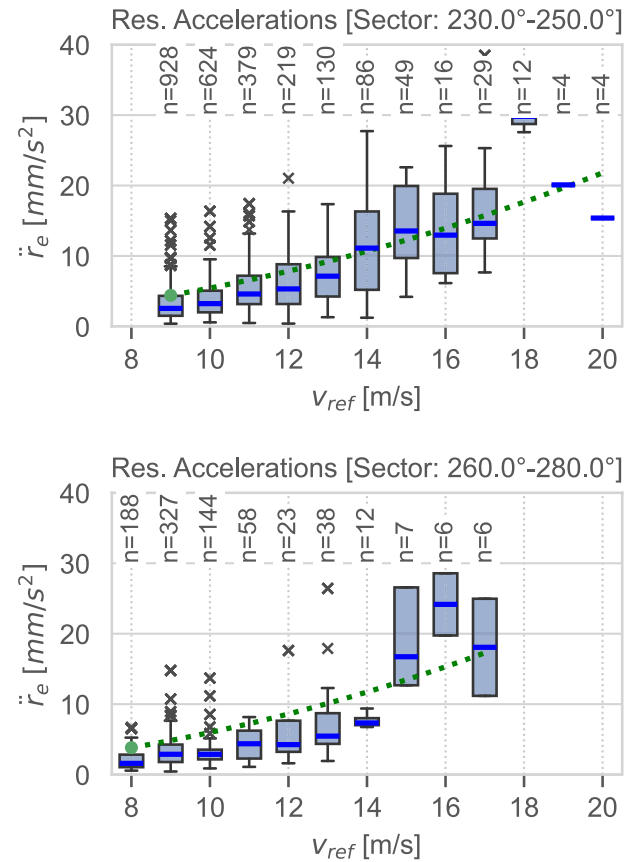
5.4. Wind conditions

The longterm analysis of the ultrasonic probe on the roof top of the building towards the (RTM) data unveils the influence of the urban context of the building, and of the building itself. In Section 3.2, the corresponding directional effects are already demonstrated. As the ultrasonic probe is partially shielded by the building (see Fig. 5, Fig. 7), inaccuracies are unavoidable. Fig. 10 presents a comparison of wind conditions as box plots, with whiskers representing the 5%–95% quantiles and outliers marked with 'x'. In Fig. 10(a), the distribution of average wind speeds over wind direction for $v_{RTM} \geq v_{cond.}$ is shown. The overall average measured at the building itself is significantly lower in the most disturbed wind sector ($\Phi = 300° - 30°$).

Wind conditions can also be reconstructed based on the pressure data, described in Section 5.1. Assuming a dominance of the turbulent wind flow on the drag coefficient, Eq. (13) is used to interpret the turbulence intensity at the height of the pressure taps. Comparison to the data of the ultrasonic probe has been used to fit the correlation parameter to $\alpha = 0.56$, assumed constant for all wind directions, showing reasonable correlation effect.

Fig. 10(b) shows significant scatter of the measured turbulence intensities, determined based on two independent sources (by the ultrasonic probe on the roof top of the building and reconstructed based on the fluctuation of c_D). While a good match of turbulence intensity can be observed for less disturbed flow directions ($\Phi = 75 - 200°$), areas influenced by neighboring structures ($\Phi = 300 - 30°$) and the building itself (ultrasonic probe) show higher turbulence values measured by the ultrasonic probe on the rooftop. Even for less disturbed flow directions, the turbulence intensity exceeds $I_v = 0.2$ on average, and a significant number of outliers have been observed, despite $v_{cond} = 8$ m/s was respected for this analysis.

(a) Comparison of mean wind speed to the RTM weather station

(b) Comparison comparison of turbulence intensity to integral pressure fluctuations (correlation effect fitted to $\alpha = 0.56$)

Fig. 10. Wind conditions during the measurement period. Comparison of ultrasonic probe on the rooftop to alternative sources.

Fig. 11. Example of x–y trajectories (tower top motion) during a 10 min event. Dashed ellipses: Mahalanobis distances of two levels of confidence (98.9% and 99.8%).

Fig. 12. Resultant peak acceleration $\ddot{r}_e$ at the building edge for two relevant wind sectors and number of events n_{event}.

5.5. Accelerations

For each time period, the detailed x-y-trajectories have been analyzed for the shape of acceleration. It was found that the motion of the building showed significant interaction between both building axes, mainly ovaling or alternating between in-wind and cross-wind vibrations (see Fig. 11). The main axes of vibrations have been determined using Singular Value Decomposition (SVD).

It was noted that the 1st and 2nd axes (resulting from SVD) are not necessarily aligned with the in-wind and cross-wind directions. Typically, the SVD axes are aligned with the main buildings axes. All datasets with $v \geq v_{cond}$ were analyzed in the time domain in the presented way to obtain trajectories and quantile values ($p = 99.8\%$) of peak accelerations and standard deviations of accelerations. The time-series obtained by the three accelerometers have been analyzed to separate the transversal and torsional accelerations, dependent on the geometrical arrangement. For a motion-direction-independent analysis, the resultant acceleration at the center of the cross-section, $\ddot{r}_c$, was calculated. To account for torsional effects, the resultant acceleration at the building edge farthest from the center of the cross-section, $\ddot{r}_e$, was also determined (see Fig. 12).

In order to derive peak accelerations based on Eq. (2), the peak factor k_p needs to be clarified. Based on the in-situ data, an analysis of peak factors has been made for each dataset with $v \geq v_{cond}$. The peak factor has been derived as ratio of the peak acceleration of the event to the standard deviation and is shown in Fig. 13.

The analysis of peak factors shows factors converging to approximately $k_p = 3.5$ (as specified in Netherlands Standardization Institute (2011)) for increasing amplitudes. In the range of lower amplitudes, significant scatter is visible. A significant relation of the peak factors to the wind direction has not been observed.
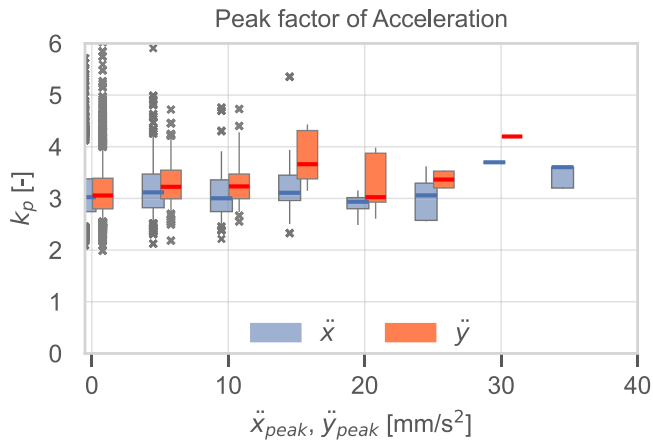
Fig. 13. Peak factor of the measured accelerations in x and y direction based on 10 min events.
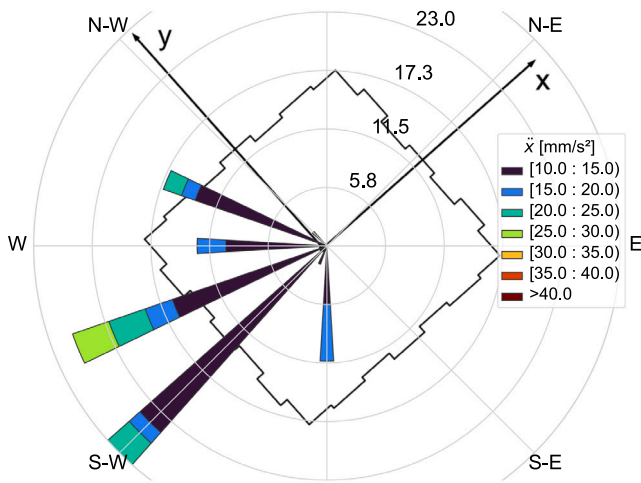

Fig. 14. Rose plot of acceleration $\ddot{x}$ dependent on wind direction.
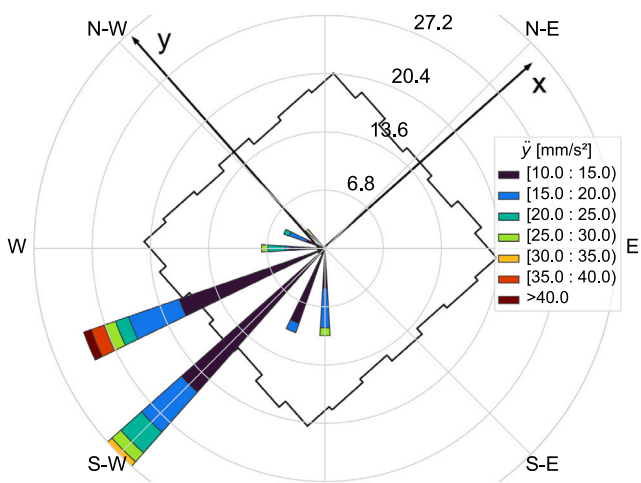

Fig. 15. Rose plot of acceleration $\ddot{y}$ dependent on wind direction.

Figs. 14 and 15 present rose plots of the measured accelerations in the x and y directions, illustrating their dependency on wind direction. The plots reveal two key findings: (1) The dominant vibration

mode of the New Orleans Tower is characterized by ovalling, indicating a continuous exchange between the two principal directions. This behavior highlights the dynamic interaction between the building's structural response and the wind-induced forces. (2) The most pronounced accelerations occur in a wind sector influenced by the upstream high-rise tower (Montevideo), suggesting that wake turbulence from this adjacent structure significantly contributes to the observed vibration amplitudes. These insights underline the importance of considering neighboring structures and their aerodynamic effects when assessing wind-induced vibrations in tall buildings.

6. Comparison of predicted and measured vibrations

Peak accelerations in tall buildings can be predicted using the framework established in Eq. (2), which relates the peak acceleration to wind conditions, structural properties, and aerodynamic influences. Since both eigenfrequencies f_x and f_y and the corresponding mode shapes Ψ_x and Ψ_y are nearly identical for the almost square-shaped building, the structural term, represented by the fraction in Eq. (1), can be considered constant for each direction and independent of wind conditions. To account for wind conditions and aerodynamic influences, the values determined in Section 5 are used for each observed event.

To ensure a comprehensive comparison, the predicted acceleration values are calculated for each time segment, considering the mean velocity (upscaled to the reference height z_s) and the directional aerodynamic properties. The analysis is performed on three levels to progressively refine the prediction accuracy.

Level 1 assumes data as typically available during the planning stage, including turbulence intensity, drag coefficient, and structural properties as specified in NEN-EN 1991-1-4 (Netherlands Standardization Institute, 2011). In Fig. 16(a), the predicted accelerations $\ddot{x}_{p,EN}$ are compared to the measured peak accelerations $\ddot{r}_e$ from all data sets. The results indicate that this model tends to overestimate a considerable number of events, resulting in a wide scatter and questioning the reliability of the prediction quality.

Level 2 introduces directional drag coefficients derived from wind tunnel tests, enhancing the predictive accuracy. As shown in Fig. 16(b), the scatter becomes more concentrated around the ideal diagonal, indicating an improved prediction. However, this refinement also reveals an increased number of underestimations.
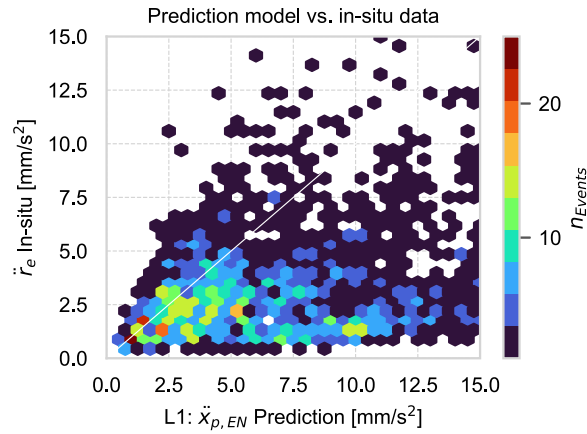
Level 3 incorporates the full set of measured data, including turbulence intensity, directional drag coefficients, and structural properties, into Eq. (1). As presented in Fig. 16(c), this approach further reduces the scatter and further improves prediction accuracy.

The visualization in Fig. 16 demonstrates that the general approach for predicting along-wind vibrations according to Method 2 (Netherlands Standardization Institute, 2011) provides realistic results, provided the input parameters are accurately determined. In particular, the consideration of local turbulence conditions and directional drag coefficients is crucial. Therefore, reliable aerodynamic data obtained from wind tunnel tests or numerical simulations is essential for accurate predictions.
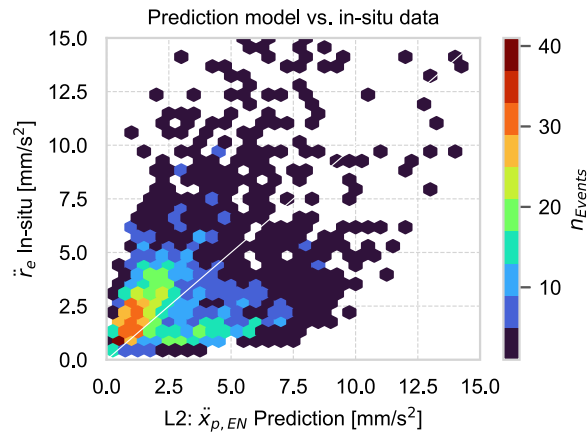
7. Comfort criterium

In Johann et al. (2015), several criteria to evaluated high-tower vibration comfort n the context of evaluating wind-induced accelerations in tall buildings are discussed. ISO 10137 provides a widely accepted framework for assessing occupant comfort. The standard establishes comfort limits based on peak accelerations for a one-year return period, differentiating between residential and office buildings. As human perception is particularly sensitive to low-frequency oscillations, the limiting amplitudes are formulated as frequency-dependent and specified here for the most relevant frequency range of tall residential buildings.
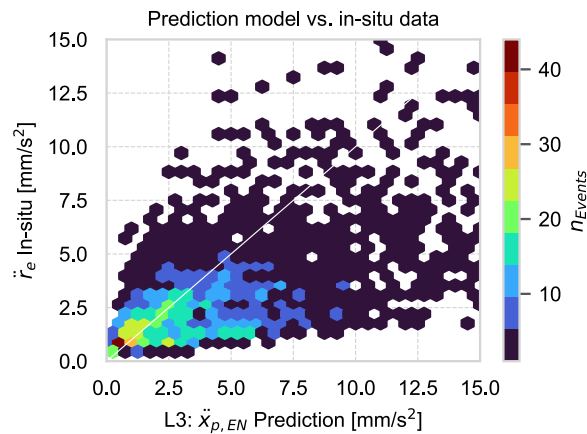
$$A(f_0) = 42.0 \cdot f_0^{-0.445} \; mm/s^2 \quad 0.06\,\text{Hz} \leq f_0 \leq 1.0\,\text{Hz} \tag{18}$$

(a) Individual wind speed (v_m) but simplified turbulence (I_v) and non-directional aerodynamic (c_D) based on standard for each event

(b) Individual wind speed (v_m) but simplified turbulence (I_v), directional aerodynamic (c_D) based on BLWT for each event

(c) Individual wind (v_m, Iv) and aerodynamic (c_D) conditions for each event

Fig. 16. Comparison of EC-M2 prediction to measured peak amplitudes of accelerations.

These criteria are based on a conservative approach, assuming that peak accelerations should not exceed the specified limits more than once per year. To better understand the building's dynamic response,
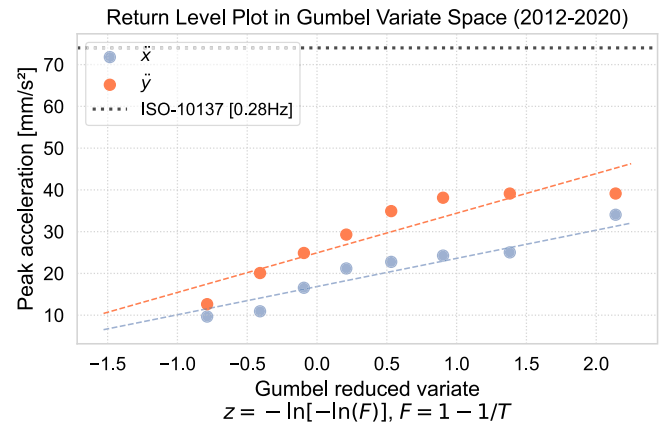

Fig. 17. Yearly extreme values of the transversal vibrations and comparison to ISO-10137 (Anon, 2007).

the measured peak accelerations from the New Orleans Tower will be compared to the ISO 10137 (Anon, 2007) limits, considering the building's fundamental frequencies and the associated comfort thresholds for residential use.

For the New Orleans Tower, the limiting acceleration amplitude based on ISO 10137 is calculated as $A(f_0 = 0.28 \text{ Hz}) = 74 \text{ mm/s}^2$, considering the lower of the two nearly identical principal eigenfrequencies. Based on all measurements that have been made, a single maximum acceleration was found with $\ddot{x} = 75 \text{ mm/s}^2$. However, that event has been identified as faulty, because the pattern of trajectories showed abrupt changes. The remaining data has been analysed with extreme value statistics and the yearly extremes for $\ddot{x}$ and $\ddot{y}$ are plotted in Fig. 17.

8. Conclusions

This study provides an in-depth analysis of gust-induced vibrations in high-rise structures, comparing in-situ measurements with prediction models based on Eurocode provisions and wind tunnel experiments. Using data from the New Orleans Tower, a detailed assessment of aerodynamic forces, structural dynamics, and environmental influences was performed to evaluate the reliability of current predictive methodologies. Key findings highlight that:

1. Code Predictions vs. Reality: Current Eurocode provisions significantly overpredict drag forces compared to in-situ measurements. This discrepancy indicates that the simplified assumptions in the Eurocode may not adequately account for complex urban flow conditions. While wind tunnel tests introduced in this study were designed conservatively using smooth flow conditions, they still provided valuable insights into refining the prediction of aerodynamic forces.
2. Influence of Neighboring Structures: Wake effects and local turbulence caused by adjacent buildings significantly impact measured responses, particularly in urban environments. The wind tunnel tests can incorporate the influence of neighboring structures, which is absent in the Eurocode framework. However, deviations between wind tunnel results and in-situ data were observed, suggesting that further refinement of the modeling process is necessary to align with real-world behavior.
3. Role of In-Situ Measurements: Real measured data is critical for validating and enhancing code provisions. This study demonstrated that incorporating measured structural and aerodynamic parameters into the predictive framework significantly improves its accuracy. In-situ measurements bridge the gap between theoretical assumptions and actual building responses, enabling meaningful advancements in design methodologies.

4. Directional Influence: The directional dependence of wind forces and their impact on structural responses is crucial in wind engineering. This study highlights the significance of directional analysis in accurately predicting vibrations. However, simplified code concepts often do not provide models capable of addressing these directional effects, limiting their predictive capability in complex urban scenarios.

While the Eurocode offers a robust framework for estimating wind-induced vibrations, this study demonstrates the necessity of integrating advanced data from wind tunnel tests and long-term monitoring campaigns. Enhanced site-specific models that consider the urban context, directional effects, and measured data are essential to improving prediction reliability. Future work will leverage high-fidelity LES and new wind-tunnel tests configured with the same urban roughness to provide matched datasets for the New Orleans tower and its surroundings. The objective is to translate these data into directional force coefficients and turbulence descriptors suitable for Method-2 predictions, thereby reducing the bias observed here and informing practical adjustments to current code provisions.

CRediT authorship contribution statement

Declaration of competing interest

The authors declare that they have no known competing financial interests or personal relationships that could have appeared to influence the work reported in this paper.

Acknowledgments

Data availability

Data will be made available on request.

References

Anon, 2005. CUR 103: Wind Tunnel Investigation for the Determination of Design Wind Loads on (Tall) Buildings and Their Components (In Dutch Language). Technical Report, Civil Engineering Centre for Research and Regulation (CUR).

Anon, 2007. ISO 10137:1992 - bases for design of structures – serviceability of buildings against vibration.

Anon, 2022. ASCE/SEI 7-22: Minimum Design Loads and Associated Criteria for Buildings and Other Structures. American Society of Civil Engineers.

Antoine, J., Olivari, D., 2009. Blockage effects in closed-section wind tunnels: a review. J. Wind Eng. Ind. Aerodyn. 97 (11–12), 514–522.

Bronkhorst, A., Geurts, C., 2020. Long-term vibration and wind load monitoring on a high-rise building. In: Proceedings ISMA2020, Leuven, Belgium.

Buresti, G., 1981. The effect of blockage and aspect ratio on the mean flow past a circular cylinder normal to the stream. J. Wind Eng. Ind. Aerodyn. 8 (1–2), 105–114.

Coyle, D., 1931. Measuring the behaviour of tall buildings. Eng. News-Record 1931, 310–313.

Dalgliesh, W.A., Cooper, K.R., Templin, J., 1983. Comparison of model and full-scale accelerations of a high-rise building. J. Wind Eng. Ind. Aerodyn. 13 (1–3), 217–228.

Davenport, A.G., 1961. A Statistical Approach to the Treatment of Wind Loading of Tall Masts and Suspension Bridges (PhD Dissertation). University of Bristle.

Davenport, A.G., 1964. Note on the distribution of the largest value of a random function with application to gust loading. Proc. Inst. Civ. Eng. 28 (2), 187–196.

Davenport, A.G., 1965. The buffeting of structures by gusts. In: Proc. of Conference on'Wind Effects on Structures', NPL, 1965, Vol. 357. ICWE-1, HMSO.

Davenport, A.G., 1967. Gust loading factors. J. Struct. Div. 93 (3), 11–34.

Eaton, K., 1971. Wind Loading on Tall Buildings (Ph.D. thesis). University College London (UCL).

Eiffel, G., 1900. Travaux scientifiques exécutés à la tour de trois cents mètres de 1889 à 1900. L. Maretheux, imprimeur.

Engineering Sciences Data Unit, 1976. Response of Flexible Structures to Atmospheric Turbulence, vol. 76001, ESDU International plc.

Jeary, A., 1978. The Dynamic Behaviour of the Arts Tower, University of Sheffield, and Its Implications to Wind Loading and Occupant Reaction. Building Research Establishment, Department of the Environment.

Johann, F.A., Carlos, M.E., Ricardo, F.L., 2015. Wind-induced motion on tall buildings: A comfort criteria overview. J. Wind Eng. Ind. Aerodyn. 142, 26–42.

Kemper, F., 2022. Prediction of gust induced cycle counts and fatigue damage of structures. J. Wind Eng. Ind. Aerodyn. 226, 105004.

Koster, T., Kalkman, I.M., Bronkhorst, A.J., 2014. Reliable Prediction of Wind Loads on High-Rise Building Façades: Wind Tunnel Measurements on the New Orleans Tower in Rotterdam. Internal Report TNO 2014 R10662, TNO, 392 pages (including appendices).

Moretti, D., Bronkhorst, A., Geurts, C., 2022. Identification of the structural properties of a high-rise building. In: Proceedings ISMA2022, Leuven, Belgium.

Netherlands Standardization Institute, 2011. Eurocode 1: Actions on structures - Part 1-4: General actions - Wind actions. NEN, Netherlands Standardization Institute, Delft, The Netherlands.

Netherlands Standardization Institute, 2023. National Annex to NEN-EN 1991-1-4+A1+C2: Eurocode 1: Actions on Structures - Part 1-4: General Actions - Wind Actions. NEN, Netherlands Standardization Institute, Delft, The Netherlands.

Rathbun, J.C., 1940. Wind forces on a tall building. Trans. Am. Soc. Civ. Eng. 105 (1), 1–41.

Simiu, E., Scanlan, R.H., 1996. Wind Effects on Structures: Fundamentals and Applications to Design, third ed. Wiley, New York.

Solari, G., Kareem, A., 1998. On the formulation of ASCE7-95 gust effect factor. J. Wind Eng. Ind. Aerodyn. 77–78, 673–684.

Steenbergen, R., Vrouwenvelder, A., Geurts, C., 2012. The use of eurocode EN 1991-1-4 procedures 1 and 2 for building dynamics, a comparative study. J. Wind Eng. Ind. Aerodyn. 107–108, 299–306.

van Bentum, C., Geurts, C., 2015. Full scale measurements of pressure equalization on air permeable façade elements. In: ICWE 14, 14th International Conference on Wind Engineering. Conference Paper.

Van Koten, H., 1971. The comparison of measured and calculated amplitudes of some buildings and determination of the damping effects of the buildings. In: Proc. 3rd Int. Conf. on Wind Effects on Buildings and Structures. pp. 825–839.